# ENDOR and Special TRIPLE Resonance Spectroscopy of $Q_A^{\bullet-}$ of Photosystem 2[†]

Stephen E. J. Rigby,[‡] Peter Heathcote,[§] Michael C. W. Evans,[‡] and Jonathan H. A. Nugent*,[‡]

*Department of Biology, Darwin Building, University College London, London, WC1E 6BT, UK, and School of Biological Sciences, Queen Mary and Westfield College, Mile End Road, London, E1 4NS, UK*

*Received January 12, 1995; Revised Manuscript Received July 10, 1995*[⊗]

ABSTRACT: ENDOR and special TRIPLE spectroscopies have been used to study the electron spin density distribution and hydrogen bonding of the plastosemiquinone anion radical, $Q_A^{\bullet-}$, of photosystem 2. The semiquinone radical was made accessible to ENDOR through the use of exogenous cyanide, which decouples the radical from the ferrous iron of the photosystem 2 ferroquinone acceptor complex [Sanakis, Y., et al. (1994) *Biochemistry 33*, 9922]. $H_2O/D_2O$ exchange was used to assign hyperfine couplings to hydrogen-bonded protons, and orientation-selected special TRIPLE spectroscopy has revealed the orientation of hydrogen bonds relative to the quinone ring. Methyl group resonances have also been assigned. ENDOR spectra of the decylplastosemiquinone anion radical *in vitro* are presented for comparison. This shows that interaction with the protein leads to changes in the electron spin density distribution and the hydrogen bond orientation; both hydrogen bonds are parallel to the quinone ring plane *in vitro*, whereas $Q_A^{\bullet-}$ has one parallel and one perpendicular to the plane. These results are discussed in the light of previous ENDOR studies of the ubiquinone radical $Q_A^{\bullet-}$ of *Rhodobacter sphaeroides* and the predicted structure of the $Q_A$-binding region of photosystem 2.

The secondary electron acceptor in both the purple bacterial photosynthetic reaction center and photosystem 2 (PS2)[1] of oxygenic photosynthesis is a ferroquinone complex, consisting of a non-heme $Fe^{2+}$ ion and a quinone designated $Q_A$ [for reviews, see Deisenhofer and Norris (1993), and Diner et al. (1991)]. The structure of the purple bacterial photosynthetic reaction center has been determined by using X-ray crystallography (Deisenhofer et al., 1985; Allen et al., 1986). This shows that, in the ferroquinone complex, the iron is coordinated by four histidine ligands and one glutamate, which acts as a bidentate ligand. $Q_A$ is menaquinone in *Rhodopseudomonas viridis* and ubiquinone in *Rhodobacter sphaeroides*. The quinone accepts an electron to become an anionic semiquinone radical ($Q_A^{\bullet-}$); the iron is not redox active under turnover conditions and exists in the high-spin ($S = 2$) state.

The situation in PS2 is somewhat different. First, there is no experimentally determined three-dimensional structure available, although the structure has been modelled wholly or in part using the purple bacterial reaction center as a basis (Michel & Deisenhofer, 1988; Svensson et al., 1990; Ruffle et al., 1992). Second, the glutamate ligand to the non-heme iron is not conserved in PS2 amino acid sequences (Deisenhofer & Michel, 1989). Third, the iron ligand environment is affected by exogenous ligands such as bicarbonate (probably the "native" ligand), formate, nitric oxide, and cyanide (Vermaas & Rutherford, 1984; Diner & Petrouleas, 1984; Koulougliotis et al., 1993). It is tempting to assume that the bicarbonate replaces the glutamate ligand of the purple bacteria, but this has yet to be shown. Last, the quinone in PS2 is plastoquinone. These data suggest that while the structure of the ferroquinone complex in PS2 is similar to that in purple bacteria, it may manifest subtle differences that can be probed spectroscopically.

Since a semiquinone radical is formed, electron paramagnetic resonance (EPR) spectroscopy should be a useful probe of the $Fe^{2+}-Q_A^{\bullet-}$ complex. This has indeed proved to be the case, with EPR providing the evidence for the effects of exogenous ligands referred to earlier. However, magnetic coupling between the semiquinone radical and the non-heme iron leads to a broad EPR spectrum (Bowden et al., 1991; Nugent et al., 1981, 1992), which principally reports changes in this coupling rather than details of the semiquinone environment. This broad spectrum also prevents the use of the related electron nuclear double-resonance (ENDOR) technique that has been used in the study of other protein-bound radical species (Dorio & Freed, 1979; Kurreck et al., 1988). The iron in the *Rb. sphaeroides* photosynthetic reaction center may be removed and replaced by a diamagnetic metal ion such as $Zn^{2+}$ (Debus et al., 1986). This has allowed an ENDOR spectroscopic study of the electronic structure of $Q_A^{\bullet-}$ in this species and its interaction with the protein (Lubitz et al., 1985). While iron removal (Klimov et al., 1980) and reconstitution with other metals has been reported (Akabori et al., 1992) for PS2, this preparation is not readily reproducible. Recently, however, it has been shown (Sanakis et al., 1994) that cyanide can convert the non-heme iron to a diamagnetic low-spin, $S = 0$, state in PS2, thus allowing for the formation of a $Q_A^{\bullet-}$ radical EPR spectrum without coupling to the iron.

Here we report an ENDOR and special TRIPLE (ST) resonance spectroscopic study of the PS2 $Q_A^{\bullet-}$ semiquinone radical formed by chemical reduction of cyanide-treated PS2

[†] We acknowledge financial support from the U.K. Biotechnology and Biological Sciences Research Council (BBSRC).

* Address correspondence to this author.

[‡] University College London.

[§] Queen Mary and Westfield College.

[⊗] Abstract published in *Advance ACS Abstracts,* September 1, 1995.

[1] Abbreviations: ENDOR, electron nuclear double-resonance spectroscopy; EPR, electron paramagnetic resonance spectroscopy; hfc, hyperfine coupling constant; d-PQ, decylplastoquinone; PS2, photosystem 2; $Q_A$, the first quinone acceptor of photosystem 2; Tris, tris(hydroxymethyl)aminomethane; $\nu_H$, proton Larmor frequency; ST, special TRIPLE resonance spectroscopy.

0006-2960/95/0434-12075$09.00/0 

and of the decylplastoquinone anion radical in alkaline isopropyl alcohol. The results are analyzed in the light of the earlier ENDOR study of $Q_A^{\bullet-}$ in *Rb. sphaeroides* (Lubitz et al., 1985) and reports of the ENDOR of $Q_A^{\bullet-}$ in iron-depleted PS2 (Macmillan et al., 1990, 1995).

## MATERIALS AND METHODS

PS2 membranes [BBYs (Berthold et al., 1981), Chl *a*/Chl *b* ratio of 2.05−2.20:1] were prepared from market spinach (*Spinacea oleracea*) by the method of Ford and Evans (1983). The Tris-washed material (depleted of manganese and the three extrinsic lumenal proteins) was prepared from BBY particles by incubation in 1 M tris(hydroxymethyl)-aminomethane hydrochloride (Tris-HCl, pH 8.8) on ice under room illumination for 1 h, followed by centrifugation at 40000*g* for 30 min at 4 °C. Tris-washed PS2 was resuspended in 50 mM Tris-HCl (pH 8.8) at 15−18 mg/mL total chlorophyll and incubated with 350 mM potassium cyanide [KCN; from a freshly made stock 3.5 M solution in 0.1 M Tris-HCl, pH 8.8] in 3 mm i.d. EPR tubes (sample volume 200 $\mu$L), in the dark, on ice for 45 min. A solution of sodium dithionite (25 $\mu$L, 115 mM, under argon in 0.1 M Tris-HCl, pH 8.8) was then added, and following another 15 min incubation on ice in the dark, the samples were frozen in liquid nitrogen in the dark. For hydrogen/deuterium exchange experiments, the Tris-washed PS2 was resuspended in 50 mM Tris-HCl (pD 8.8)/$D_2O$ at ca. 0.2 mg/mL total chlorophyll and centrifuged for 30 min at 40000*g*. The pellet was resuspended in a small volume of the $D_2O$ buffer as before at 15−18 mg/mL total chlorophyll and loaded into 3 mm i.d. EPR tubes. These samples were then incubated at 4 °C for 16 h in the dark prior to the addition of cyanide and dithionite as before.

The anionic semiquinone of decylplastoquinone (2,3-dimethyl-5-decyl-1,4-benzoquinone, Sigma Chemical Company) was produced by sodium borohydride reduction of a 3.5 mM solution of quinone in alkaline isopropyl alcohol under argon (Hales & Case, 1981). The samples for ENDOR spectroscopy were frozen in 3 mm i.d. EPR tubes in liquid nitrogen under a stream of argon.

ENDOR, ST, and EPR spectra were obtained at X-band using a Bruker ESP 300 EPR spectrometer, as described in Rigby et al. (1994a,b). Spectra were corrected for a small baseline nonlinearity by the subtraction of off-resonance scans, which were filtered for noise (standard Bruker software) to avoid reducing the spectrum signal to noise ratio. The experimental spectra were not filtered for noise. Acquisition conditions for specific spectra are given in the figure captions. Characteristic ENDOR and ST line shapes were established by examining several sets of samples involving different PS2 preparations. The precision of hfc determination, i.e., the variation in hfc determination between these samples, was ±0.05 MHz. Spectra are presented in first-derivative mode. The hyperfine coupling constants are measured from zero crossing points, except for $A_{||}$ features where the peak maximum is used.

## RESULTS

Figure 1a shows the EPR spectrum in the $g = 2.00$ region of the species formed by dithionite reduction of cyanide-treated PS2. The signal occurs at $g = 2.0045$ and is 0.95 mT wide (peak to peak). The $g$ value is typical of anionic

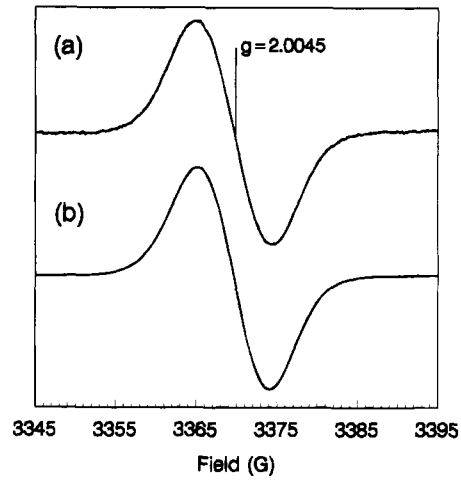


FIGURE 1: (a) EPR spectrum of $Q_A^{\bullet-}$ in dithionite-reduced, cyanide-treated, Tris-washed BBY membranes (see Materials and Methods) at 100 K. (b) EPR spectrum of the decylplastoquinone anion radical (d-$PQ^{\bullet-}$) in isopropyl alcohol, prepared as in Materials and Methods, at 120 K. Experimental conditions: microwave power, 50 $\mu$W; modulation amplitude, 1.2 G; modulation frequency, 12.5 kHz. (a) is the sum of two scans; recorded in the ENDOR cavity.

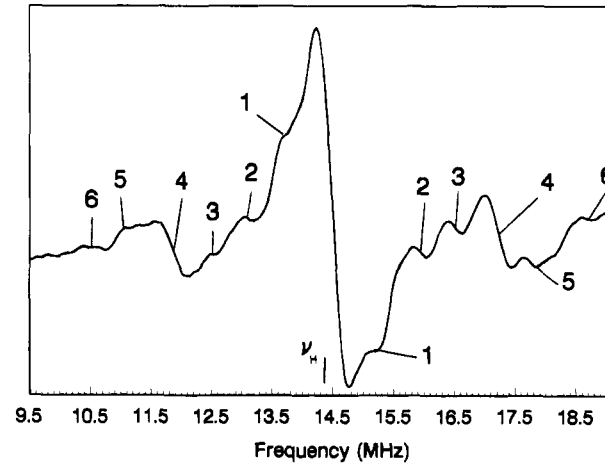


FIGURE 2: Broad sweep ENDOR spectrum of $Q_A^{\bullet-}$ in cyanide-treated, Tris-washed BBY membranes (see Materials and Methods) at 100 K. Numbers refer to resonances assigned in Table 1. Experimental conditions: microwave power, 4.9 mW; radiofrequency power, 100 W; radiofrequency modulation depth, 200 kHz; scan time, 84 s; time constant, 655 ms; sum of 120 scans.

semiquinone radicals (Burghaus et al., 1993), and the properties of the signal are the same as those reported recently by Sanakis et al. (1994). The dark-stable tyrosine radical in PS2, termed $Y_D^{\bullet}$, was removed by the cyanide treatment. Comparison at nonsaturating microwave powers of an untreated sample, strongly illuminated at room temperature and then frozen to 77 K to induce maximum $Y_D^{\bullet}$ (about 1 spin per reaction center), with the $Q_A^{\bullet-}$ in a treated sample of equal PS2 concentration showed that $Q_A^{\bullet-}$ was present in 80 ± 5% of centers, which is very similar to estimates by previous workers (Sanakis et al., 1994). We therefore assign this signal to the anionic semiquinone radical of the secondary electron acceptor $Q_A$.

The ENDOR spectrum of $Q_A^{\bullet-}$ is shown in Figure 2. ENDOR resonances in this region arise from hyperfine coupling to protons. The most prominent features of semiquinone frozen solution ENDOR spectra are expected to arise from hyperfine coupling to the protons of methyl groups attached to the quinone ring (O'Malley & Babcock,

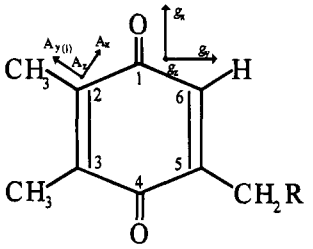


FIGURE 3: Structure of plastoquinone showing the carbon atom numbering scheme and the relative orientation of the hyperfine (**A**), and **g** tensors. The $z$ direction is perpendicular to the page. For plastoquinone-9, R = solanesyl, i.e., $CHC(CH_3)CH_2(CH_2CHC(CH_3)CH_2)_9H$.

1984) and protein protons hydrogen bonded to the quinone oxygens (O'Malley & Babcock, 1986). From the structure of plastoquinone (Figure 3), a maximum of two methyl group and two H-bond (one to each oxygen) hyperfine couplings (hfcs) are expected. Both these types of couplings give rise to axial resonances in ENDOR spectra, with a strong $A_\perp$ feature and a weaker $A_\parallel$ turning point. The three protons of the methyl groups are rendered equivalent by methyl group rotation. Features 2−4 of Figure 2 show the line shapes and intensities expected of methyl group or H-bond $A_\perp$ components. Feature 5 has the line shape expected of an $A_\parallel$ component while the weak feature 6 may arise from the methylene protons at position 5. The resolved feature 1 arises from hyperfine coupling to a proton(s) of the protein matrix.

Relatively high temperatures (100 K) are necessary for the detection of the $Q_A$ ENDOR spectrum, reflecting the relatively long electron spin relaxation time of the unpaired electron in the absence of dipolar interactions with the high-spin form of the ferrous iron or the oxygen-evolving complex. Such temperatures lead to a rather poor signal to noise ratio due to a disadvantageous Boltzmann distribution. The signal to noise ratio has been increased in Figure 2 through the use of high modulation depths, but at the expense of resolution. To enable lower modulation depths to be employed, leading to higher spectral resolution, but without a signal to noise penalty, we have used the ST resonance technique (Figure 4) (Freed, 1969; Dinse et al., 1974). This is a variation on the ENDOR technique using two radiofrequency fields and one microwave field, which produces "half-spectra" with greater intensity than those from standard ENDOR. The origin (0 MHz) corresponds to the center of the ENDOR spectrum (Larmor frequency), and therefore the line positions can be read off directly as $A/2$. Our spectrometer only allows ST from 1 MHz, and therefore feature 1 and part of feature 2 are lost due to their proximity to the spectrum origin. The ST spectrum of $Q_A$ is shown in Figure 4a. The enhanced sensitivity of the ST technique has revealed a new feature (feature 7) that has the line shape expected of an hfc $A_\parallel$ component.

Hyperfine coupling to hydrogen-bonded protons may be distinguished by recording the spectra of samples that have been exchanged into $D_2O$. Such a spectrum is shown in Figure 4b. Features 2, 4, and 7 are absent from this spectrum, and therefore these features can be assigned to the $A_\perp$ (features 2 and 4) and $A_\parallel$ (feature 7) components of hyperfine couplings to hydrogen-bonded protons. Features 4 and 7 follow the relationship $2A_\perp \approx A_\parallel$ and are therefore assigned as the perpendicular and parallel components of

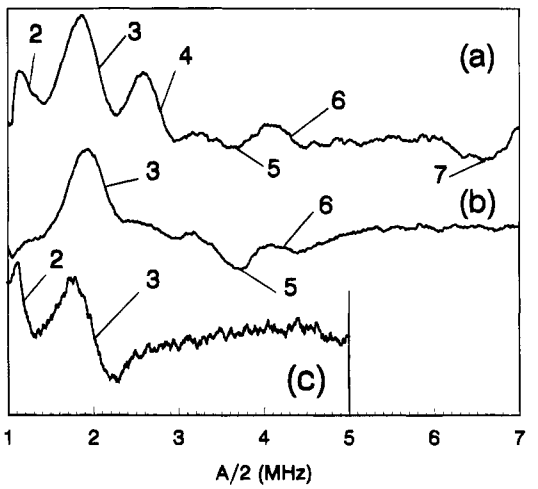


FIGURE 4: ST spectra of $Q_A^{\bullet-}$ in cyanide-treated, Tris-washed BBY membranes at 100 K: (a) powder spectrum in $H_2O$ buffer; (b) powder spectrum in $D_2O$ buffer; (c) part of the $z$-oriented spectrum in $H_2O$ buffer recorded at a field 7 G upfield of the EPR crossing point. Numbers refer to resonances assigned in Table 1. Experimental conditions: microwave power, 4.9 mW; radiofrequency power, 200 W (total over both channels); radiofrequency modulation depth, 100 kHz; scan time, 84 s; time constant, 655 ms; sum of 160 scans.

the same hyperfine coupling. The resulting isotropic hfc calculated from these two components is +0.3 MHz, which is comparable with the +0.1 MHz reported for benzosemiquinone anion radical (O'Malley & Babcock, 1986). Features 3 and 5 are unaffected by $D_2O/H_2O$ exchange and therefore are presumed to arise from the $A_\perp$ and $A_\parallel$ components, respectively, of a methyl group hfc. The insensitivity of feature 6 to solvent exchange supports the assignment of this feature to a covalently bonded proton of the quinone, possibly a methylene proton of the solanesyl group at position 5. The hfcs of $\beta$-methylene protons are dependent on both the spin density at the attached carbon atom and the orientation of the methylene group relative to the ring (Heller & McConnell, 1960; Rigby et al., 1994a). Thus, the hfcs of such protons may be much larger than those of methyl groups attached to the same ring.

The orientation of the hydrogen bond relative to the quinone is not defined by the quinone structure, but rather by its binding site in the protein. This orientation may be determined by using orientation selection ENDOR. The EPR powder spectrum is the sum of spectra arising from electron spins at all possible orientations to the magnetic field. Where the **g** tensor is anisotropic, however, the edges of the EPR spectrum (i.e., at field values corresponding to $g_z$ or $g_x$) arise from electron spins for which the **g** tensor is oriented along the $z$ or $x$ axes. Therefore, by acquiring ENDOR (or ST) spectra at field values corresponding to the edges of the EPR spectrum, specific orientations of molecules in the **g** tensor coordinate frame may be studied (Rist & Hyde, 1968; O'Malley & Babcock, 1986). ENDOR of such specifically oriented molecules no longer produces a powder spectrum, but rather the specific components of the ENDOR spectrum arising from the orientation-selected ENDOR spectra acquired at the high-field ($g_z$) edge of the EPR spectrum will show the $z$ components (in the **g** tensor coordinate frame) of asymmetric hyperfine tensors. In a previous study of the PS2 tyrosine radical $Y_D^{\bullet}$ (Rigby et al., 1994a), we used orientation selection to isolate both the $z$ and $x$ components

of hyperfine tensors. However, the **g** tensors of semiquinone anion radicals have been shown by high-field EPR (Burghaus et al., 1993) to be almost axial ($g_x = 2.0063$, $g_y = 2.0052$, and $g_z = 2.0023$ for the plastosemiquinone anion *in vitro*), and therefore it is not possible to select the $x$ orientation without some contribution from the $y$ orientation. Thus, only the $z$ orientation, which may be selected without interference, is employed in this study.

Here we have used orientation-selected ST spectroscopy (Figure 4c) to improve the signal to noise ratio of the resulting spectrum. Despite the signal to noise advantages of ST, however, only the intense $A_\perp$ components of the axial hyperfine couplings are visible due to the decreased EPR intensity at the edge of the spectrum. The ST spectrum of $Q_A^{\bullet-}$ taken 0.7 mT upfield of the EPR crossing point (i.e., close to $g_z$) is shown in Figure 4c. From the relative orientations of the **g** and hyperfine tensor axes (Figure 3), it can be seen that the methyl group $A_z$ and the $g_z$ axes are collinear and that both axes are perpendicular to the quinone ring plane. Since the parallel component of the methyl group hyperfine coupling is directed up the ring carbon−methyl carbon bond (Figure 3), the $A_z$ component of this coupling is one of the two perpendicular components. Therefore, the $A_z$ component of the methyl group coupling should be observed in Figure 4c, and this is indeed the case. Note that the change in the line shape of feature 3 on going from the powder to the orientation-selected spectrum of Figure 4c leads to a small shift (0.05 MHz) in the position of this feature. Feature 4, the H-bond $A_\perp$, is not observed, showing that for this hfc the $g_z$ axis is collinear with the parallel axis of the hyperfine coupling, i.e., that the H-bond is oriented perpendicularly to the quinone ring plane. The poor signal to noise ratio of spectra taken at $g_z$ precluded the observation of the H-bond $A_\parallel$ feature (feature 7) even by ST spectroscopy, and that part of the spectrum encompassing feature 7 is not shown in Figure 4c.

The origin of feature 2 has yet to be determined. Although part of it can be seen in Figure 4, the hyperfine coupling of this feature places it too close to the origin of the ST spectrum for accurate observation. Therefore, despite the signal to noise disadvantage, ENDOR spectra in $H_2O$, $D_2O$, and $H_2O$ taken at $g_z$ have been acquired over a range sufficient to include features 1 and 2 (Figure 5). Comparison of Figure 5 parts a and b shows that feature 2 disappears upon exchange into $D_2O$, and therefore this feature is assigned to the $A_\perp$ component of a hyperfine coupling to a hydrogen-bonded proton. This is supported by the behavior of the part of feature 2 that is visible in Figure 4. The $A_\parallel$ component of this coupling would be at approximately twice the $A_\perp$ value and would fall under feature 4. The spectrum acquired at $g_z$ (Figure 5c) shows that feature 2 is observed at this orientation, which places the hydrogen bond parallel to the plane of the quinone ring. The presence of part of feature 2 in Figure 4c is consistent with this orientation. It is possible that this hyperfine coupling has no axes that are coincident with the axes of the **g** tensor, in which case its orientation cannot be determined from the data of Figure 5. However, the failure to observe an $A_\parallel$ component for this coupling in Figure 4c at 5.5−6.0 MHz suggests that the H-bond in question truly is perpendicular to the $z$ direction. This identifies all the features in the spectrum, and from these assignments it follows that both methyl groups of $Q_A^{\bullet-}$ have the same hyperfine coupling, represented by features 3 and 5. The hyperfine coupling constants determined for $Q_A^{\bullet-}$ are collected in Table 1.

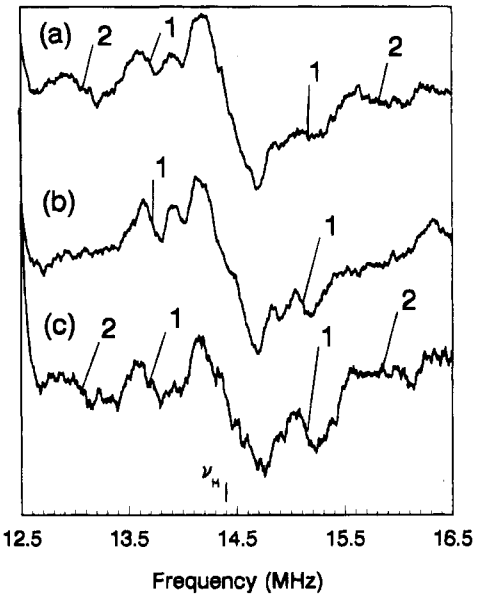


FIGURE 5: ENDOR spectra of $Q_A^{\bullet-}$ in cyanide-treated, Tris-washed BBY membranes at 100 K, covering the matrix region to show features 1 and 2: (a) powder spectrum in $H_2O$ buffer; (b) powder spectrum in $D_2O$ buffer; (c) $z$-oriented spectrum in $H_2O$ buffer, recorded at a field 7 G upfield of the EPR crossing point. Numbers refer to resonances assigned in Table 1. Experimental conditions: microwave power, 3.9 mW; radiofrequency power, 50 W; radiofrequency modulation depth, 60 kHz; scan time, 84 s; time constant, 655 ms; sum of 100 scans.

Table 1: Hyperfine Coupling Constants (MHz)[a] and Resonance Assignments for $Q_A^{\bullet-}$ and the Decylplastoquinone Anion Radical ($PQ^{\bullet-}$) in Isopropyl Alcohol

| feature | $Q_A^{\bullet-}$ | $PQ^{\bullet-}$ | assignment |
|---|---|---|---|
| 1 | 1.5 | | matrix |
| 2 | −2.7 | −2.6 | H-bond $A_\perp$ |
| 3 | 4.1 | 3.6 | methyl $A_\perp$ |
| 3A | | 4.9 | methyl $A_\perp$ |
| 4 | −5.6 | −4.9 | H-bond $A_\perp$ |
| 5 | 7.3 | | methyl $A_\parallel$ |
| 6 | 8.6 | 8.1 | $\beta$-CH $A_\perp$ |
| 7 | 13.1 | | H-bond $A_\parallel$ |

[a] The attribution of negative signs to the perpendicular components of hydrogen bond couplings follows from Muto and Iwasaki (1973) and O'Malley and Babcock (1986).

The EPR spectrum of the decylplastosemiquinone anion radical (d-$PQ^{\bullet-}$) is shown in Figure 1b. The $g$ value (2.0045) and line width (0.95 mT) are the same as those of the $Q_A^{\bullet-}$ radical. The ENDOR spectrum of d-$PQ^{\bullet-}$ has also been obtained and may be assigned using the same arguments applied to $Q_A^{\bullet-}$ earlier. Decylplastoquinone replaces the unsaturated solanesyl group at position 5 with a saturated decyl group. Since the unpaired electron is delocalized into the $\pi$-orbital system of the benzoquinone structure, this substitution does not affect the electron spin density distribution detected by ENDOR. In the following discussion and Figures 6 and 7, the resonance numbering scheme employed for the analysis of the $Q_A^{\bullet-}$ spectra is maintained for ease of comparison; thus, features with the same number are assigned to hfcs to the same protons in the structure (see also Table 1). Figure 6 shows the spectra of d-$PQ^{\bullet-}$ in protonated and deuterated isopropyl alcohol taken at the EPR crossing point, and Figure 7 shows spectra taken at $g_z$. From

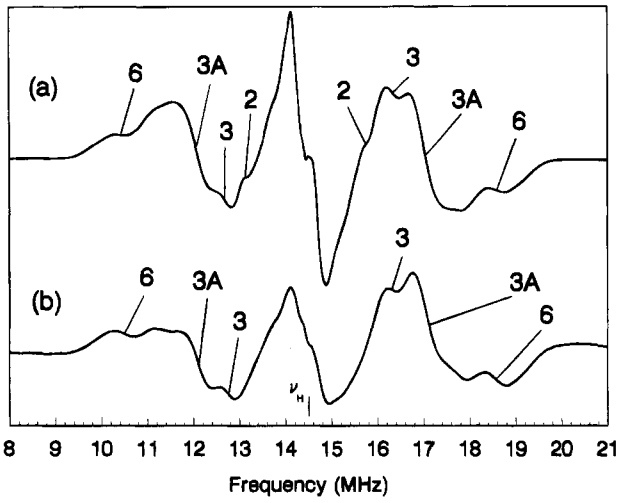


FIGURE 6: ENDOR spectra of the decylplastoquinone anion radical ($PQ^{\bullet-}$), prepared as in Materials and Methods, at 120 K in (a) isopropyl alcohol and (b) isopropyl alcohol-*OH-d*). Numbers refer to resonances assigned in Table 1. Experimental conditions: microwave power, 7.9 mW; radiofrequency power, 63 W; radiofrequency modulation depth, 80 kHz; scan time, 84 s; time constant, 655 ms; sum of 30 scans.

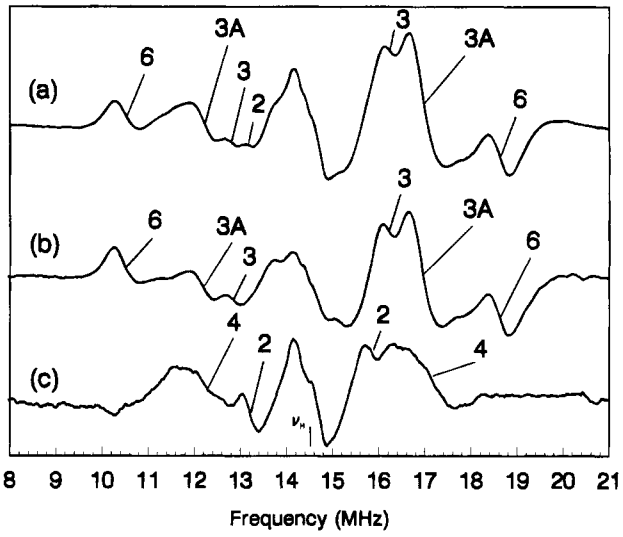


FIGURE 7: *z*-oriented ENDOR spectra of the decylplastoquinone anion radical ($PQ^{\bullet-}$) at 120 K in (a) isopropyl alcohol and (b) isopropyl alcohol-*OH-d*) and (c) the difference spectrum of (a) minus (b). Numbers refer to resonances assigned in Table 1. Experimental conditions as Figure 7, except they are a sum of 60 scans.

these spectra, feature 2 and an underlying component of feature 3 (Figure 6a) are assigned as hydrogen bond $A_\perp$ components since they are not present in the spectrum taken in deuterated solvent (Figure 6b). From their line shapes and intensities, features 3 and 3A (which are not affected in deuterated solvent) are assigned as the partially resolved $A_\perp$ components of the hyperfine couplings to the methyl groups at positions 2 and 3 (see Figure 3). The H-bond giving rise to feature 2 is oriented parallel to the quinone ring plane since this feature is present in the *z*-oriented spectrum (Figure 7). The reduction in intensity of feature 3 in the *z*-oriented spectra (Figure 7a,b) on going from protonated to deuterated solvent suggests that the H-bond providing the underlying intensity of feature 3 is parallel to the quinone ring plane. This feature is resolved in the difference spectrum (Figure 7c, feature 4). Feature 6 is also present in the *z*-oriented spectra, indicating that this too is an $A_\perp$ component of a quinone substituent hyperfine coupling, possibly to a methylene proton at position 5. The $A_\parallel$ components of the methyl group couplings are expected to occur between features 3 and 4 and account for the decrease in intensity of this region on going from powder to *z*-oriented spectra. $A_\parallel$ components for the H-bond hyperfine couplings have not been observed, but can be estimated on the basis that hydrogen bond couplings are approximately traceless, i.e., $A_\parallel \simeq 2A_\perp$ (Muto & Iwasaki, 1973). The hyperfine coupling constants of d-$PQ^{\bullet-}$ are collected in Table 1.

## DISCUSSION

Comparison of the hyperfine couplings of $Q_A^{\bullet-}$ with those of d-$PQ^{\bullet-}$ reveals differences between the two radicals. First, the hyperfine couplings of the methyl groups at positions 2 and 3 of $Q_A^{\bullet-}$ are identical, whereas there is a 1.3 MHz difference between the methyl group couplings of d-$PQ^{\bullet-}$. The $Q_A^{\bullet-}$ methyl group coupling is in fact close to the mean average of the two d-$PQ^{\bullet-}$ couplings. Since methyl group hfcs report the electron spin density at the attached (ring) carbon (McConnell, 1956), this observation suggests that interaction with the protein causes a more symmetrical distribution of electron spin density between carbons 2 and 3. Second, although the hydrogen bond hyperfine couplings have similar magnitudes in the two species, $Q_A^{\bullet-}$ has one hydrogen bond perpendicular to the ring plane, an orientation not observed for hydrogen bonds to d-$PQ^{\bullet-}$. Whether the differences in H-bond orientation are responsible for the observed changes in methyl group hfcs is not clear, as other quinone–protein interactions may affect the methyl group hfcs in $Q_A^{\bullet-}$. Only small differences between $Q_A^{\bullet-}$ and d-$PQ^{\bullet-}$ might be expected, as the difference in $E_m$ between them is only ca. 30 mV (Knaff, 1975), suggesting that the electronic structure of the quinone is not greatly perturbed upon binding to the protein. A stoichiometry of 2 $CN^-$ per PS2 would be expected if the monodentate cyanide ligands replace the bidentate bicarbonate in the PS2 non-heme iron coordination sphere. Therefore, the observation of Sanakis et al. (1994) that up to three cyanide ions may bind per PS2 raises the possibility that the cyanide treatment itself may perturb the $Q_A$-binding site by replacing one of the histidine ligands to the iron. However, the binding sites for these cyanide ions have yet to be located, and they may not all bind to the non-heme iron.

ENDOR studies of $PQ^{\bullet-}$ and $Q_A^{\bullet-}$ in iron-depleted PS2 have been reported previously by Macmillan et al. (1990). Their solution state study of $PQ^{\bullet-}$ in isopropyl alcohol gave methyl group isotropic hfcs ($A_{iso}$) of 4.81 and 5.49 MHz. By taking $A_\parallel - A_\perp$ for semiquinones in frozen solution to be ca. 3 MHz (O'Malley & Babcock, 1984), the methyl group $A_{iso}$ values obtained from our frozen solution study are 4.6 and 5.9 MHz, which are in reasonable agreement with the solution state studies of Macmillan et al. Such small differences between frozen and liquid solution hfcs have been reported previously for 2,5-dimethylsemiquinone, 1,2,4,5-tetramethylsemiquinone (O'Malley & Babcock, 1984), and ubisemiquinone-10 (Das et al., 1970; Lubitz et al., 1985). The frozen solution ENDOR spectrum of $PQ^{\bullet-}$ reported in Macmillan et al. (1990), however, is assigned very different methyl group hfcs, with $A_\perp = 6.8$ MHz, $A_\parallel = 9.8$ MHz ($A_{iso} = 7.8$ MHz) and $A_\perp = 3.0$ MHz, $A_\parallel = 4.1$ MHz ($A_{iso} = 3.4$ MHz). We have found no precedent for such extreme

differences between liquid and frozen solution ENDOR spectra of the same semiquinone. Macmillan et al. suggest that these differences may be caused by asymmetric hydrogen bonding, but offer evidence of only one H-bond hfc (obtained using deuterated solvent). The study of $Q_A^{\bullet-}$ consists of a single ENDOR spectrum with low signal to noise ratio, perhaps as a result of heterogeneity at the $Q_A$ site induced by demetalation. This spectrum is assigned solely by comparison with the above mentioned frozen solution spectrum of $PQ^{\bullet-}$. Thus, without resolution of the discrepancies between the liquid and frozen solution assignments presented in Macmillan et al. (1990) for $PQ^{\bullet-}$, it is impossible to comment on their $Q_A^{\bullet-}$ assignments.

It should be noted that in a subsequent poster communication (Macmillan et al., 26th International ESR Conference, Sheffield, U.K., 1993) a frozen solution spectrum of $PQ^{\bullet-}$ was presented with suggested H-bond $A_\perp$ components of 2.57 and 5.10 MHz and a methyl group hfc characterized by $A_\perp$ = 4.33 MHz and $A_\parallel$ = 6.7 MHz, with no equivalent of the large methyl hfc reported in the earlier communication (Macmillan et al., 1990). The spectrum of $Q_A^{\bullet-}$ in iron-depleted PS2 presented at this time (Macmillan et al., (1990) suggested H-bond hfc $A_\perp$ components of 2.85 and 5.71 MHz, with a methyl group hfc characterized by $A_\perp$ = 4.23 MHz and $A_\parallel$ = 7.30 MHz. The values for both radicals are consistent with those we report here. Recently, the same research group presented a more thorough study of $PQ^{\bullet-}$ and $Q_A^{\bullet-}$ in iron-depleted PS2 (Macmillan et al., 1995) using Q-band EPR and X-band ENDOR. This study largely agrees with ours except in the assignment of feature 4, which Macmillan et al. assign as a H-bond $A_\parallel$ component paired with an $A_\perp$ component of ca. −1 MHz. The assigment of feature 4 to an $A_\parallel$ component seems incompatible with the line shapes that we observe for this feature, particularly in Figure 4. They do not observe an hfc equivalent to our feature 7. Their small $A_\perp$ component at −0.85 MHz for $PQ^{\bullet-}$ may arise from the use of fully deuterated isopropyl alcohol as solvent rather than the isopropyl alcohol-*OH-d* employed here, allowing hfcs to solvent protons other than the H-bonding solvent OH proton to appear in H minus D difference spectra.

Comparison with the earlier ENDOR study of the quinone acceptor in zinc-substituted *Rb. sphaeroides* reaction centers (Lubitz et al., 1985) is not easy since there the quinone is ubiquinone-10. The methyl group hyperfine coupling of $Q_A^{\bullet-}$ in PS2 is very similar to that reported for the equivalent radical in *Rb. sphaeroides* ($A_\perp$ = 4.0 MHz, $A_\parallel$ = 7.1 MHz). However, the *Rb. sphaeroides* H-bond hfcs are very different: $A_\perp$ = 4.7 MHz, $A_\parallel$ = 9.0 MHz and $A_\perp$ = 6.4 MHz with an undetected $A_\parallel$. Note that it was also reported that when DDQ (2,3-dimethoxy-5,6-dimethylquinone) binds at the $Q_A$ site in *Rb. sphaeroides* the methyl group hfcs of the DDQ anion radical are not equivalent (Lubitz et al., 1985). This stands in contrast to the behavior of the two methyl group hfcs of $Q_A^{\bullet-}$. Therefore, the quinone−protein interactions in PS2 may differ from those in *Rb. sphaeroides,* as sequence comparisons suggest.

$Q_A$ is located by homology modeling (Ruffle et al., 1992; Ruffle & Nugent, 1992) to the loop between transmembrane helices 4 and 5 of D2. D2 residues located near $Q_A$ include L211, H215, T218, W254, F258, F262, and L268 (Figure 8). W254 is in van der Waals contact with both $Q_A$ and the active branch pheophytin intermediate electron carrier, which

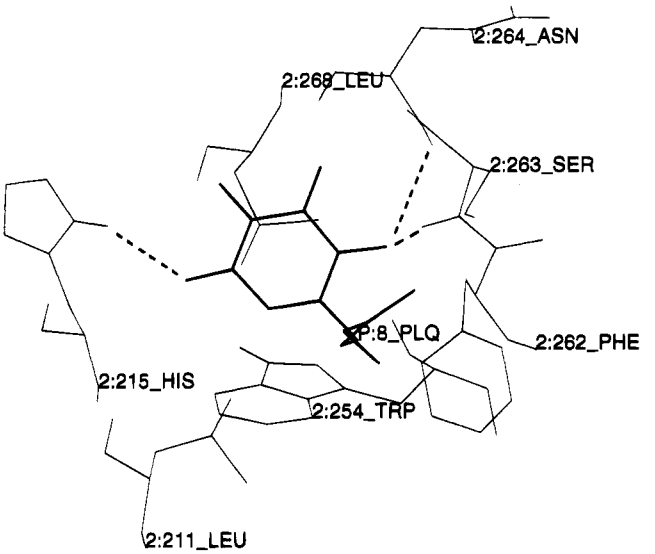


FIGURE 8: $Q_A$-binding region of the D2 polypeptide taken from the model of photosystem 2 (Ruffle et al., 1992). Possible hydrogen bonds are indicated by the dashed lines.

suggests that it functions to facilitate electron transfer between pheophytin and $Q_A$. The model suggests several possible interactions between D2 and $Q_A$. The carbonyl group closest to the non-heme iron can form two possible hydrogen bonds. One of these is to the non-heme iron ligand, H215, and the other is to T218. The other quinone carbonyl group could hydrogen bond to the main chain of two residues, S263 and N264. Studies on mutations that affect the $Q_A$ hydrogen bonds should help identify the residues involved.

For plastoquinone radicals it is not clear whether the difference between the two H-bond hfcs arises from differences in the O−H distance or the unpaired electron spin density at the quinone oxygens. If the oxygen electron spin densities are equivalent, then the O−H distance is given by (Feher et al., 1988)

$$r \propto (1/A_\perp)^{1/3}$$

Therefore, the H-bond giving rise to the smaller hfcs (feature 2) is 1.3 times the length of the H-bond corresponding to the larger hfcs (features 4 and 7). At present, it is not clear which H-bond hfcs involve which oxygen atom. It is possible that, at least for d-$PQ^{\bullet-}$ *in vitro*, steric crowding by the C(3)-methyl and C(5)-decyl groups may limit the access of solvent to the C(4)-oxygen, leading to a longer O−H distance for the H-bond to the C(4)-oxygen. The lengths and orientations of H-bonds to $Q_A^{\bullet-}$ are functions of the $Q_A$-binding pocket in PS2 rather than a property of the quinone, and thus no conclusions can be drawn concerning the assignment of hfcs to a particular H-bonded oxygen.

We are currently extending our ENDOR and ST studies to the second quinone acceptor of PS2, $Q_B$, in order to delineate the differences in the quinone-binding sites of PS2 that lead to the differing properties of $Q_A$ and $Q_B$.

## ACKNOWLEDGMENT

The authors thank Prof. W. Lubitz for the preprint of Macmillan et al. (1995).

## REFERENCES


Akabori, K., Kuroiwa, S., & Toyoshima, Y. (1992) in *Research in Photosynthesis* (Murata, N., Ed.) Vol. II, p 123, Kluwer Academic Publishers, Dordrecht, The Netherlands.

Allen, J. P., Feher, G., Yeates, T. O., Rees, D. C., Deisenhofer, J., Michel, H., & Huber, R. (1986) *Proc. Natl. Acad. Sci. U.S.A. 83*, 8589.

Berthold, D. A., Babcock, G. T., & Yocum, C. F. (1981) *FEBS Lett. 134*, 231.

Bowden, S. J., Hallahan, B. J., Ruffle, S. V., Evans, M. C. W., & Nugent, J. H. A. (1991) *Biochim. Biophys. Acta 1060*, 89.

Burghaus, O., Plato, M., Rohrer, M., Möbius, K., MacMillan, F., & Lubitz, W. (1993) *J. Phys. Chem. 97*, 7639.

Das, M. R., Connor, H. D., Leniart, D. S., & Freed, J. H. (1970) *J. Am. Chem. Soc. 92*, 2258.

Debus, R. J., Feher, G., & Okamura, M. Y. (1986) *Biochemistry 25*, 2276.

Deisenhofer, J., & Michel, H. (1989) *EMBO J. 8*, 2149.

Deisenhofer, J., & Norris, J. R. (1993) *The Photosynthetic Reaction Center Vols. 1&2*, Academic Press, San Diego.

Deisenhofer, J., Epp, O., Miki, R., Huber, R., & Michel, H. (1985) *Nature (London) 318*, 618.

Diner, B. A., & Petrouleas, V. (1990) *Biochim. Biophys. Acta 1015*, 141.

Diner, B. A., Petrouleas, V., & Wendoloski, J. J. (1991) *Physiol. Plant. 81*, 432.

Dinse, K. P., Biehl, R., & Möbius, K. (1974) *J. Chem. Phys. 61*, 4335.

Dorio, M. M., & Freed, J. H. (1979) *Multiple Electron Resonance Spectroscopy*, Plenum Press, New York.

Feher, G., Isaacson, R. A., Okamura, M. Y., & Lubitz, W. (1988) in *The Photosynthetic Bacterial Reaction Center: Structure and Dynamics* (Breton, J., & Vermeglio, A., Eds.) pp 229–235, Plenum Press, New York.

Ford, R. C., & Evans, M. C. W. (1983) *FEBS Lett. 160*, 159.

Freed, J. H. (1969) *J. Chem. Phys. 50*, 2271.

Hales, B. J., & Case, E. E. (1981) *Biochim. Biophys. Acta 637*, 291.

Klimov, V. V., Dolan, E., Shaw, E. R., & Ke, B. (1980) *Proc. Natl. Acad. Sci. U.S.A. 77*, 7227.

Knaff, D. B. (1975) *FEBS Lett. 60*, 331.

Koulougliotis, D., Kostopoulos, T., Petrouleas, V., & Diner, B. A. (1993) *Biochim. Biophys. Acta 1142*, 275.

Kurreck, H., Kirste, B., & Lubitz, W. (1988) *Electron Nuclear Double Resonance Spectroscopy of Radicals in Solution: Application to Organic and Biological Chemistry*, VCH Publishers, Weinheim, Germany.

Lubitz, W., Abresch, E. C., Debus, R. J., Isaacson, R. A., Okamura, M. Y., & Feher, G. (1985) *Biochim. Biophys. Acta 808*, 464.

Macmillan, F., Gleiter, H., Renger, G., & Lubitz, W. (1990) in *Current Research in Photosynthesis* (Baltscheffsky, M., Ed.) Vol. I, p 531, Kluwer Academic Publishers, Dordrecht, The Netherlands.

Macmillan, F., Lendzian, F., Renger, G., & Lubitz, W. (1995) *Biochemistry 34*, 8144–8156.

McConnell, H. M. (1956) *J. Chem. Phys. 24*, 764.

Michel, H., & Deisenhofer, J. (1988) *Biochemistry 27*, 1.

Muto, H., & Iwasaki, M. J. (1973) *J. Chem. Phys. 59*, 4821.

Nugent, J. H. A., Diner, B. A., & Evans, M. C. W. (1981) *FEBS Lett. 124*, 241.

Nugent, J. H. A., Doetschman, D. C., & Maclachlan, D. J. (1992) *Biochemistry 31*, 2935.

O'Malley, P. J., & Babcock, G. T. (1984) *J. Chem. Phys. 80*, 3912.

O'Malley, P. J., & Babcock, G. T. (1986) *J. Am. Chem. Soc. 108*, 3995.

Rigby, S. E. J., Nugent, J. H. A., & O'Malley, P. J. (1994a) *Biochemistry 33*, 1734.

Rigby, S. E. J., Nugent, J. H. A., & O'Malley, P. J. (1994b) *Biochemistry 33*, 10043.

Rist, G. H., & Hyde, J. S. (1968) *J. Chem. Phys. 49*, 2449.

Ruffle, S. V., & Nugent, J. H. A. (1992) *Research in Photosynthesis* (Murata, N., Ed.) Vol. II, p 191, Kluwer Academic Publishers, Dordrecht, The Netherlands.

Ruffle, S. V., Donnelly, D., Blundell, T. L., & Nugent, J. H. A. (1992) *Photosynth. Res. 34*, 287.

Sanakis, Y., Petrouleas, V., & Diner, B. A. (1994) *Biochemistry 33*, 9922.

Svensson, V., Vass, I., Cedergren, E., & Styring, S. (1990) *EMBO J. 9*, 2051.

Vermaas, W. F. J., & Rutherford, A. W. (1984) *FEBS Lett. 175*, 243.


BI950080X